

Research paper

Plastome characteristics and species identification of Chinese medicinal wintergreens (*Gaultheria*, Ericaceae)Yan-Ling Xu ^a, Hao-Hua Shen ^a, Xin-Yu Du ^{b, **}, Lu Lu ^{a,*}^a School of Pharmaceutical Sciences and Yunnan Key Laboratory of Pharmacology for Natural Products, Kunming Medical University, Kunming, Yunnan, China^b Germplasm Bank of Wild Species, Kunming Institute of Botany, Chinese Academy of Sciences, Kunming, Yunnan, China

ARTICLE INFO

Article history:

Received 12 April 2022

Received in revised form

1 June 2022

Accepted 13 June 2022

Available online 23 June 2022

Keywords:

DNA barcodes

Gene duplication

Plastome

Repeat sequences

Structural variation

ABSTRACT

Wintergreen oil is a folk medicine widely used in foods, pesticides, cosmetics and drugs. In China, nine out of 47 species within *Gaultheria* (Ericaceae) are traditionally used as Chinese medicinal wintergreens; however, phylogenetic approaches currently used to discriminating these species remain unsatisfactory. In this study, we sequenced and characterized plastomes from nine Chinese wintergreen species and identified candidate DNA barcoding regions for *Gaultheria*. Each *Gaultheria* plastome contained 110 unique genes (76 protein-coding, 30 tRNA, and four rRNA genes). Duplication of *trnFM*, *rps14*, and *rpl23* genes were detected, while all plastomes lacked *ycf1* and *ycf2* genes. *Gaultheria* plastomes shared substantially contracted SSC regions that contained only the *ndhF* gene. Moreover, plastomes of *Gaultheria leucocarpa* var. *yunnanensis* contained an inversion in the LSC region and an IR expansion to cover the *ndhF* gene. Multiple rearrangement events apparently occurred between the *Gaultheria* plastomes and those from several previously reported families in Ericales. Our phylogenetic reconstruction using 42 plastomes revealed well-supported relationships within all nine *Gaultheria* species. Additionally, seven mutational hotspot regions were identified as potential DNA barcodes for Chinese medicinal wintergreens. Our study is the first to generate complete plastomes and describe the structural variations of the complicated genus *Gaultheria*. In addition, our findings provide important resources for identification of Chinese medicinal wintergreens.

Copyright © 2022 Kunming Institute of Botany, Chinese Academy of Sciences. Publishing services by Elsevier B.V. on behalf of KeAi Communications Co., Ltd. This is an open access article under the CC BY-NC-ND license (<http://creativecommons.org/licenses/by-nc-nd/4.0/>).

1. Introduction

Gaultheria Kalm ex L. (Ericaceae), containing approximately 288 species, are widespread throughout continental areas and islands bordering the Pacific Rim (Lu et al., 2019b; Kron et al., 2020). Some *Gaultheria* species are commonly called wintergreens because they produce wintergreen oil (methyl salicylate), which is widely used in drugs, pesticides, cosmetics, and foods (Nikolić et al., 2013; Aruna et al., 2014; Luo et al., 2018). In China, nine out of 47 *Gaultheria* species are widely used as Chinese medicinal wintergreens and traditional medicine by more than nine ethnic minorities (Lu et al., 2019a; Fritsch and Lu, 2020; our own

field investigations in 2007). *Gaultheria* species are polyphyletic and include *G. fragrantissima* Wall., *G. griffithiana* Wight, *G. hookeri* C.B. Clarke, *G. leucocarpa* var. *yunnanensis* (Franch.) T.Z. Hsu & R.C. Fang, *G. longibracteolata* R.C. Fang, *G. nummularioides* D. Don, *G. pyrolifolia* J.D. Hooker ex C.B. Clarke, *G. semi-infra* (C.B. Clarke) Airy-Shaw, and *G. sinensis* Anth. These species, which all contain methyl salicylate, usually possess a distinct, mint-like aroma (Liu et al., 2013). Some species are also used in the production of Chinese herbal prescriptions, e.g., *G. leucocarpa* var. *yunnanensis* is used to produce essential balm, and *G. fragrantissima* is used in the production of "oil of Indian wintergreen" (Ma et al., 2001; Liu et al., 2013).

Chinese medicinal wintergreen plants differ in the type and content of chemical components, for instance, the content of wintergreen oil (Mukhopadhyay et al., 2016; Luo et al., 2021), but are not easily distinguished by morphological characteristics, particularly when processed into a pharmaceutical preparation. For example, one class of components that varies among Chinese medicinal

* Corresponding author.

** Corresponding author.

E-mail addresses: duxinyu@mail.kib.ac.cn (X.-Y. Du), lulukmu@163.com (L. Lu).

Peer review under responsibility of Editorial Office of Plant Diversity.

wintergreens includes lignan glucosides, which have the highest content in *G. leucocarpa* var. *yunnanensis* and are known to possess strong anti-arthritis activity (Ma et al., 2001, 2002; Cheng et al., 2009; Hu et al., 2020). In addition, *G. longibracteolata* is used to treat pulmonary heart disease due to its unique phosphodiesterase-4 (PDE4). However, misidentification of *G. longibracteolata* for *G. leucocarpa* var. *yunnanensis* or *G. fragrantissima* has resulted in the misuse of *G. longibracteolata* to treat rheumatism and inflammation (Luo et al., 2021). This misuse of wintergreen plants may decrease medicinal effects or even cause medical malpractice. Therefore, accurate species identification of Chinese medicinal wintergreens is necessary.

Previous pharmaceutical studies on wintergreens have mainly focused on the chemical compositions and their pharmacological actions (Ma et al., 2001, 2002; Liu et al., 2013; Li et al., 2017; Luo et al., 2018; Zhang et al., 2020), whereas precise species identification is often neglected. Phylogenetic analysis has placed these nine *Gaultheria* species into three clades (Fritsch et al., 2011; Zhang et al., 2017; Lu et al., 2019a): the Gymnobotrys clade (*G. leucocarpa* var. *yunnanensis*), the Trichophyllae clade (*G. sinensis*), and the Leucothoides clade (seven other species). However, this analysis based on multiple-genes (including ITS, *matK*, *rpl16*, *trnL-trnF* and *trnS-trnG*) has failed to resolve the position of seven species within the Leucothoides clade, which likely due to polyploidy, hybridization/introgression, or recent radiation (Lu et al., 2010, 2019a). Similarly, four universal DNA barcodes (i.e., ITS, *matK*, *trnH-psbA*, and *rbcL*) were unable to provide species-level discrimination in most *Gaultheria*, particularly among Chinese medicinal wintergreens (Ren et al., 2011). In contrast to a multiple-gene approach, using plastid genomes (plastomes) as DNA barcodes have been extensively adopted to provide increased numbers of DNA markers for taxonomically difficult taxa (Mwanzia et al., 2020; Lv et al., 2022).

The rapid development of high-throughput sequencing technology (Moore et al., 2006) has increased the availability of plastomes and lead to improved phylogenetic resolution at the interspecific level for many genera, e.g., *Acacia*, *Atractylodes*, *Rhododendron* and *Salvia* (Williams et al., 2016; Wang et al., 2021; Wu et al., 2021a; Fu et al., 2022). Zhang et al. (2017) resolved the inter-specific relationships of 19 species of the series *Trichophyllae* within *Gaultheria*, in which one medicinal wintergreen, *G. sinensis*, is phylogenetically placed. However, this study failed to obtain the complete plastid genome from long PCR sequences due to the presence of long repeats of a certain size, which hinder plastid genome assemblies of most species within Ericaceae (Fajardo et al., 2013; Li et al., 2020; Fu et al., 2022). Structural variations in plastome, including IR expansion or contraction, inversion, and gene duplication or loss, together with DNA sequences can be used as effective tools for plant phylogenetic analyses (Ahmed et al., 2013; Daniell et al., 2016; Liu et al., 2020). Moreover, mutations in plastomes are usually concentrated in certain regions that form mutation ‘hotspots’ (Dong et al., 2012), suggesting that plastome sequences can be used to exploit short DNA barcodes and markers. To date, complete plastid genomes and plastome structural variation in *Gaultheria* have yet to be elucidated.

In this study, we sequenced the plastid genomes of 42 individuals from all nine recognized medicinal wintergreen species within *Gaultheria*. The aims of this study were to (1) resolve phylogenetic relationships among the nine Chinese medicinal wintergreen species; (2) investigate the structural variation of plastid genomes in *Gaultheria* at both the population and species levels; and (3) propose potential DNA barcodes for future wintergreen species identification.

2. Materials and methods

2.1. Plant materials, DNA extraction, and sequencing

A total of 42 samples of Chinese medicinal wintergreens were collected in China. These samples represent nine species within *Gaultheria* and have distinct distributions. Species identification was primarily based on morphological characteristics and geological distribution. Specifically, we collected six samples of *G. fragrantissima* (LL20, LL25, LL26, LL27, X4, and X5), five samples of *G. griffithiana* (LL45, LL47, X16, X17, and X18), four samples of *G. hookeri* (LL28, LL29, X8, and X9), nine samples of *G. leucocarpa* var. *yunnanensis* (LL59, LL61, LL63, LL65, LL66, X26, X27, X28, and X29), two samples of *G. longibracteolata* (LL67 and X20), six samples of *G. nummularioides* (LL39, LL41, LL42, LL43, X11, and X14), four samples of *G. pyrolifolia* (LL33, LL34, LL35, and LL36), three samples of *G. semi-infra* (LL50, LL51, and X19) and three samples of *G. sinensis* (XX26, XX27, and XX40). Fresh leaves of each sample were collected in the field and immediately dried with silica gel for subsequent DNA extraction. Voucher specimens were preserved at the herbarium of Kunming Institute of Botany (KUN), and detailed information of the plant samples are presented in Table 1.

Genomic DNA was extracted using the modified CTAB method (Doyle and Doyle, 1987), and the quality and quantity of genomic DNA were checked. The Illumina HiSeq 2500 platform was used to sequence the 500 bp insert-size libraries and to generate 2–3 Gb pair-end reads of 150 bp in length for each sample.

2.2. Assembly, annotation, and validation of complex repeat regions

To assemble the clean reads (processed reads) into complete plastomes, *de novo* assembly was performed with the GetOrganelle toolkit (Jin et al., 2020b). Connection and annotation were subsequently conducted using Bandage 0.8.1 (Wick et al., 2015) and Geneious 9.1.4 (Biomatters Ltd., Auckland, New Zealand) with *Vaccinium macrocarpon* Aiton. (GenBank accession number: NC019616) used as the reference. Notably, some plastid regions could not be disentangled in Bandage 0.8.1 (Wick et al., 2015) due to complex or long-size repeats (Fig. 1). These regions were subsequently verified by PCR and Sanger sequencing, using newly designed primers (Table S1).

2.3. Detection of SSRs and repeat sequences

REPuter software (Kurtz et al., 2001) was used to identify forward (F), reverse (R), palindrome (P), and complementary (C) repeats in the resultant plastomes with the setting of a minimum repeat size of 30 bp and 90% or greater sequence identity (Hamming Distance = 3). Tandem Repeats Finder v.4.04 (Benson, 1999) was used to detect tandem repeats in the plastomes, with parameters set to 30 bp for the minimum repeat length, 0% for maximum mismatches and excluding repeats up to 10 bp longer than contained repeats. Simple sequence repeats (SSRs) were predicted using MISA (Beier et al., 2017) with the parameters of mono-, di-, tri-, tetra-, penta- and hexa-nucleotides set as 10, 5, 4, 3, 3, and 3, respectively. The maximum length of the sequence between two SSRs to register as a compound SSR was set to 0 bp.

2.4. Structural variation of *Gaultheria* plastomes

To investigate the structural characteristics of the *Gaultheria* plastomes under a broader scale, we downloaded representative plastomes from six related families within Ericales (i.e., Ericaceae, Lecythidaceae, Pentaphylacaceae, Primulaceae, Styracaceae and

Table 1Characteristics and voucher information of 42 novel plastomes from *Gaultheria*.

Sample	Size (bp)	LSC (bp)	SSC (bp)	IR (bp)	GC (%)	GenBank accession number	Voucher information
<i>G. fragrantissima</i> LL20	176,230	107,783	3509	32,469	36.6	OM009272	LL-060027-KUN
<i>G. fragrantissima</i> LL25	176,146	107,710	3434	32,501	36.6	OM009273	LL-0607-KUN
<i>G. fragrantissima</i> LL26	176,212	107,738	3508	32,483	36.6	OM009274	LL-0602-KUN
<i>G. fragrantissima</i> LL27	176,270	107,834	3434	32,501	36.6	OM009275	LL-S.N.-KUN
<i>G. fragrantissima</i> X4	176,230	107,783	3509	32,469	36.6	OM009276	LL-202002-KUN
<i>G. fragrantissima</i> X5	176,254	107,783	3531	32,470	36.6	OM009277	LL-202022-KUN
<i>G. griffithiana</i> LL45	178,045	107,415	3642	33,494	36.6	OM048894	LL-06100-KUN
<i>G. griffithiana</i> LL47	178,128	107,473	3597	33,529	36.6	OM048893	LL-S.N.-KUN
<i>G. griffithiana</i> X16	178,089	107,441	3572	33,538	36.6	OM048892	LL-201331-KUN
<i>G. griffithiana</i> X17	178,116	107,468	3572	33,538	36.6	OM048891	LL-201357-KUN
<i>G. griffithiana</i> X18	178,116	107,491	3617	33,504	36.6	OM048890	LL-201362-KUN
<i>G. hookeri</i> LL28	175,265	106,831	3432	32,501	36.6	OM048889	LL-07089-KUN
<i>G. hookeri</i> LL29	176,287	107,835	3510	32,471	36.6	OM048888	LL-031500-KUN
<i>G. hookeri</i> X8	176,230	107,800	3488	32,471	36.6	OM048887	LL-201619-KUN
<i>G. hookeri</i> X9	175,306	106,872	3432	32,501	36.6	OM048886	LL-201813-KUN
<i>G. leucocarpa</i> var. <i>yunnanensis</i> LL59	179,173	106,807	76	36,145	36.7	OM084803	LL-201701-KUN
<i>G. leucocarpa</i> var. <i>yunnanensis</i> LL61	179,842	107,439	137	36,133	36.6	OM084804	LL-201707-KUN
<i>G. leucocarpa</i> var. <i>yunnanensis</i> LL63	179,970	107,567	137	36,133	36.6	OM084805	LL-201205-LUN
<i>G. leucocarpa</i> var. <i>yunnanensis</i> LL65	179,841	107,438	137	36,133	36.6	OM084806	LJ-Liu1001-KUN
<i>G. leucocarpa</i> var. <i>yunnanensis</i> LL66	179,122	106,756	76	36,145	36.7	OM084807	HJ-He001-KUN
<i>G. leucocarpa</i> var. <i>yunnanensis</i> X26	179,121	106,745	78	36,149	36.6	OM084800	LL-201936-KUN
<i>G. leucocarpa</i> var. <i>yunnanensis</i> X27	179,914	107,364	140	36,205	36.6	OM084801	LL-202025-KUN
<i>G. leucocarpa</i> var. <i>yunnanensis</i> X28	179,802	107,399	137	36,133	36.6	OM084802	LL-202037-KUN
<i>G. leucocarpa</i> var. <i>yunnanensis</i> X29	182,430	107,408	124	37,449	36.6	OM084808	LL-202039-KUN
<i>G. longibracteolata</i> LL67	176,749	107,764	3503	32,741	36.5	OM048885	LL-202045-KUN
<i>G. longibracteolata</i> X20	176,637	107,848	3473	32,658	36.5	OM048884	LL-202024-KUN
<i>G. nummularioides</i> LL39	176,229	107,766	3435	32,514	36.6	OM048883	LL-07010-KUN
<i>G. nummularioides</i> LL41	176,229	107,766	3435	32,514	36.6	OM048882	LL-201143-KUN
<i>G. nummularioides</i> LL42	176,200	107,698	3432	32,535	36.6	OM048881	LL-0618A-KUN
<i>G. nummularioides</i> LL43	176,229	107,766	3435	32,514	36.6	OM048880	QD-2006-KUN
<i>G. nummularioides</i> X11	176,189	107,729	3432	32,514	36.6	OM048879	LL-201457-KUN
<i>G. nummularioides</i> X14	174,337	107,340	3089	31,954	36.7	OM048878	LL-201815-KUN
<i>G. pyrolifolia</i> LL33	175,895	107,523	3538	32,417	36.6	OM048877	LL-07117-KUN
<i>G. pyrolifolia</i> LL34	175,895	107,523	3538	32,417	36.6	OM048876	LL-07117-KUN
<i>G. pyrolifolia</i> LL35	175,895	107,523	3538	32,417	36.6	OM048875	LL-07161-KUN
<i>G. pyrolifolia</i> LL36	175,895	107,523	3538	32,417	36.6	OM048874	LL-07161-KUN
<i>G. semi-infra</i> LL50	175,905	107,498	3477	32,465	36.6	OM048870	LL-06103-KUN
<i>G. semi-infra</i> LL51	175,982	107,471	3491	32,465	36.6	OM048869	LL-06QQ-KUN
<i>G. semi-infra</i> X19	175,916	107,509	3491	32,458	36.6	OM048868	LL-201455-KUN
<i>G. sinensis</i> XX26	176,659	107,426	2585	33,324	36.7	OM048873	LL-201428-KUN
<i>G. sinensis</i> XX27	176,632	107,395	2573	33,332	36.7	OM048872	LL-201802-KUN
<i>G. sinensis</i> XX40	176,749	107,500	2585	33,332	36.7	OM048871	LL-202106-KUN

Theaceae; detailed information is provided in Table S2), and compared the structure of these plastomes with our newly generated plastomes using the MAUVE plug-in in Geneious (Darling et al., 2004).

2.5. Phylogenetic analyses

We downloaded three plastomes of the genus *Vaccinium* as outgroups (*Vaccinium bracteatum* GenBank No.: LC521967, *V. uliginosum*, LC521968 and *V. vitis-idaea*, LC521969). MAFIT v.7.310 (Katoh and Standley, 2013) was used to align the plastome sequences. Gene-partitioned model estimated using PartitionFinder2 (Lanfear et al., 2017) were used in the maximum-likelihood (ML) and Bayesian inference (BI) analyses. ML analysis was conducted using IQ-tree 1.6.12 (Nguyen et al., 2015) with support values estimated by 10,000 ultrafast bootstrap replicates. BI analysis was conducted using MrBayes 3.2.6 (Ronquist et al., 2012). Two runs with four chains were performed in parallel for ten million generations, with trees being sampled every 1000 generations.

2.6. DNA barcodes screening

The nucleotide diversity of 42 plastomes from nine species was calculated based on sliding window analysis using DnaSP v.5.10 (Librado and Rozas, 2009), with the window length set to 600 bp and step size set to 100 bp. Regions with high Pi values (> 0.2) were

picked out initially and checked within Geneious v.8.1.7 (Kearse et al., 2012) with PCR success rates considered. The selected regions at this stage were subsequently used in phylogenetic tree reconstruction using RAxML (Stamatakis, 2014). The discriminability of DNA barcodes was evaluated by reconstructing phylogenetic trees. Species in monophyly with a support rate greater than 80% was considered to be identified successfully (Barrett et al., 2016).

3. Results

3.1. Characteristics of plastomes of the Chinese medicinal wintergreens

The plastomes of all sampled *Gaultheria* share a typical quadripartite structure (Fig. 2), with GC content ranging from 36.5% to 36.7%. The plastomes ranged from 174,337 bp to 182,430 bp, with the LSC region ranging from 106,745 bp to 107,848 bp, the SSC region from 76 bp to 3642 bp, and the IR regions from 31,954 bp to 37,449 bp (Table 1). The total number of annotated genes was 137 in all samples of *G. fragrantissima*, *G. hookeri*, *G. longibracteolata*, *G. nummularioides*, *G. pyrolifolia*, *G. semi-infra* and two samples of *G. griffithiana* (LL50 and LL51), whereas it was 135 in all samples of *G. sinensis*, one sample of *G. griffithiana* (X19), and 138 in all samples of *G. leucocarpa* var. *yunnanensis*.

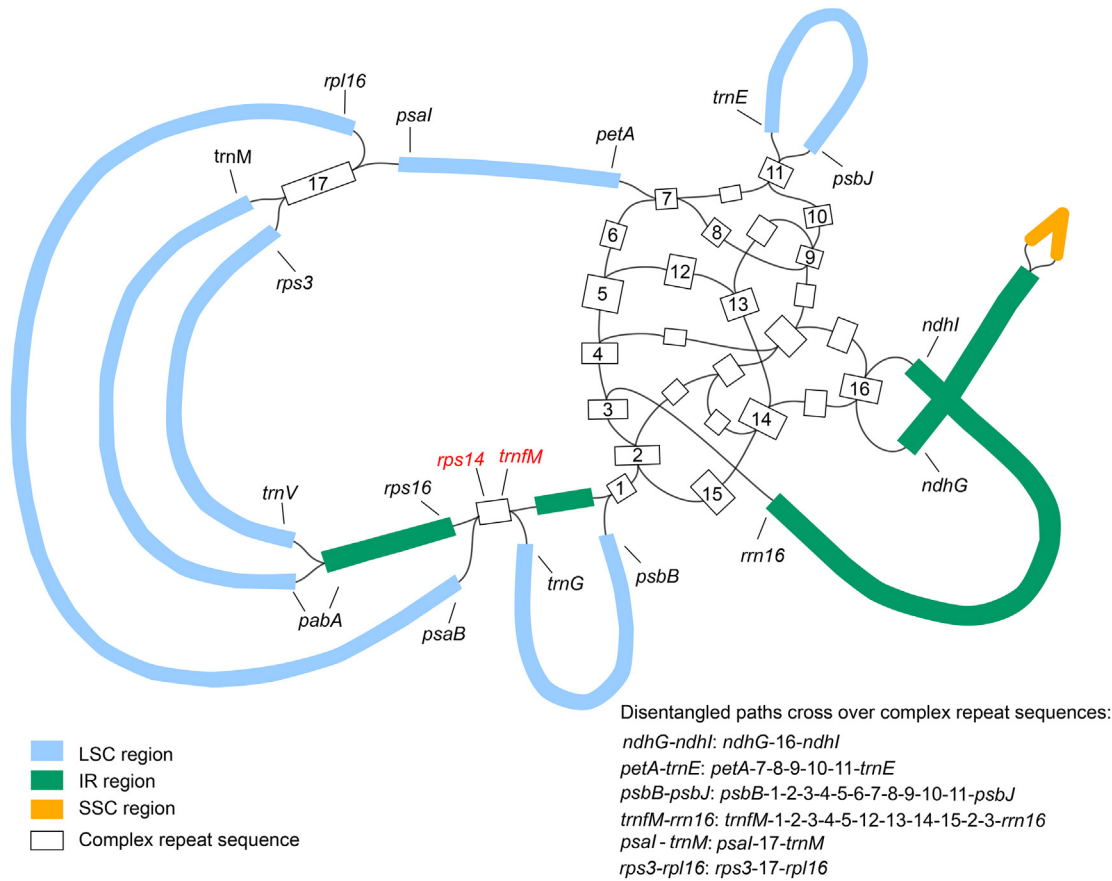


Fig. 1. Schematic diagram showing complex repeat sequences observed in the assembly graph of *de novo* assembled *Gaultheria* plastomes. The paths cross over complex repeat sequences are indicated.

Although the total number of chloroplast genes differed, the number of unique genes in each plastome was identical. Each plastome encoded 110 unique genes, including 76 protein-coding, 30 tRNA and 4 rRNA genes. All the *Gaultheria* plastomes have substantially enlarged IR regions, and the SSC region contains only one *ndhF* gene; moreover, the IR region of all samples of *G. leucocarpa* var. *yunnanensis* also contain the *ndhF* genes. We annotated two extra copies of the *rpl23* gene (not identical in sequences) in the IR regions of all *Gaultheria* plastomes except the samples of *G. sinensis* and one sample of *G. griffithiana* (X19). We also annotated two extra identical copies of the adjacent *trnfM* and *rps14* genes in the IR regions, and one extra copy of the *trnfM* gene in the LSC region (not identical in sequence) in all *Gaultheria* plastomes.

3.2. IR boundary shifts and genome comparison

We aligned all the resultant plastomes to investigate the expansion and contraction of IR boundaries. The plastomes showed high stability at the IR/LSC boundaries but were more varied at IR/SSC boundaries. The *psbA* gene spanned the IRb/LSC junction, with 236 bp on the LSC side adjacent to the *matK* gene and 826 bp on the IRb side adjacent to the *trnH* gene. For the IRa/LSC junction, the *trnV* gene was located in the LSC region 51–63 bp away from the junction, whereas the *trnH* gene was located in the IRa region 1175–1179 bp away from the junction. The boundaries of IR/SSC regions can be classified into two types. Type I: the *ndhF* gene was located in the SSC region, 15–261 bp away from the IRb/LSC

boundaries and 261–1296 bp away from IRa/SSC boundaries. This boundary type was observed in all sampled *Gaultheria* species except *G. leucocarpa* var. *yunnanensis* (Fig. 2). Type II: the *ndhF* genes were located in the IR regions due to IR expansion, and located 256–313 bp away from the IRb/SSC junction and 256–313 bp away from the IRa/SSC junction; no genes were present in the SSC region (Fig. 2). This boundary type was only observed in all samples of *G. leucocarpa* var. *yunnanensis*. Moreover, six out of nine samples of *G. leucocarpa* var. *yunnanensis* (incl., LL59, LL66, X26, X27, X28 and X29) had a unique inversion from the *psbJ* gene to the *trnE-UUC* gene (about 14 kb in length) in the LSC region, which resulted in the adjacencies of *psbJ* with *petA* and *trnE-UUC* with *psbB* (Fig. 2).

In addition, we compared the plastome structure of *Gaultheria* with plastomes from Ericaceae and five other families of Ericales (Lecythidaceae, Pentaphylacaceae, Primulaceae, Styracaceae, and Theaceae; Table S2). We found that the gene order of *Gaultheria* plastomes was collinear with *Vaccinium* (Ericaceae) but not collinear with that of *Rhododendron* (Ericaceae) (Fig. 3). The gene order of plastomes from five families of Ericales, excluding Ericaceae, are collinear (Fig. 3); however, the gene orders among *Gaultheria*, *Rhododendron*, and those five families can be explained by more than ten inversions (Fig. 3).

3.3. SSRs and long repeat sequence

A total of 2740 SSRs were identified across the 42 wintergreen plastomes (Table S3). The number of SSRs in each plastome of

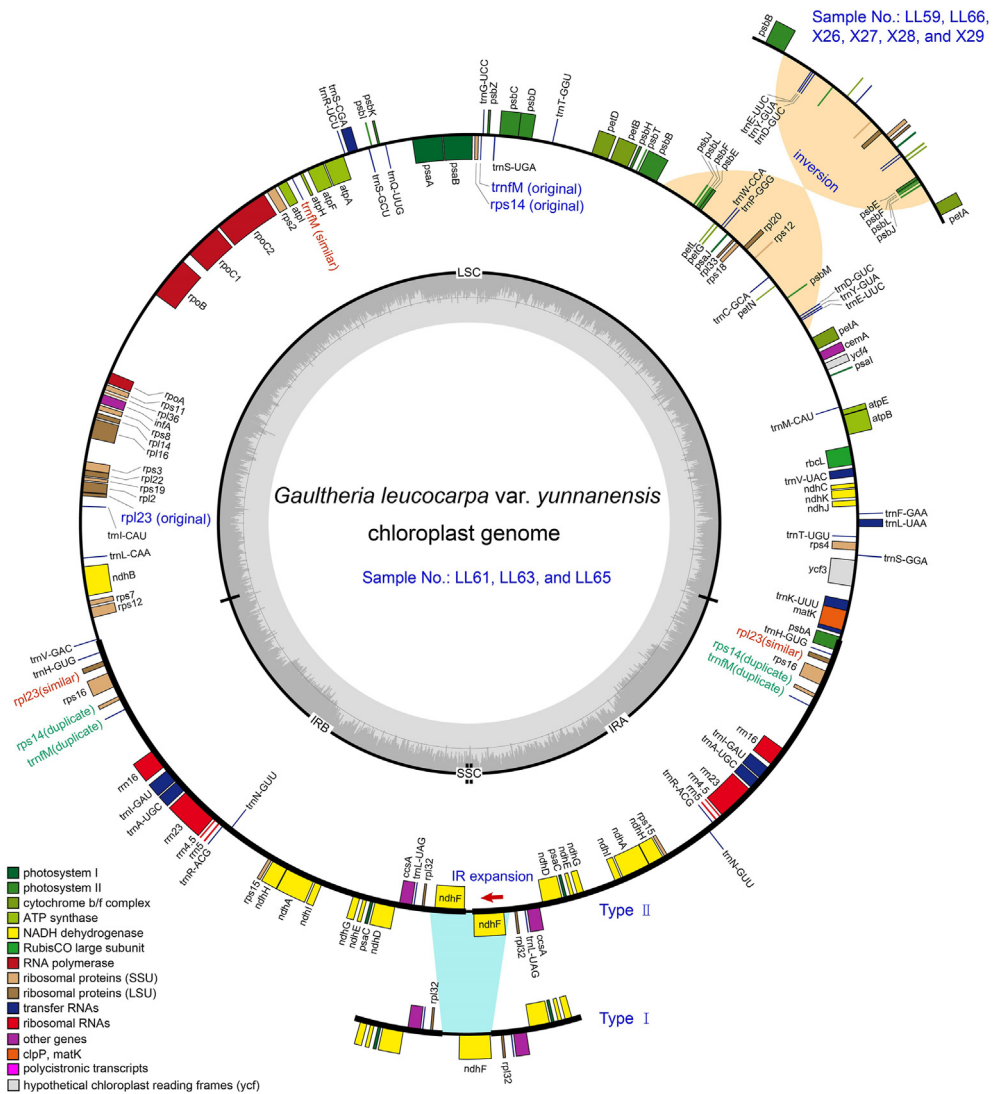


Fig. 2. Schematic plastome maps of Chinese medicinal wintergreens (*Gaultheria*). There are two basic plastome structure types. Type I: the plastomes of eight species, with the *ndhf* gene located in the SSC region (indicated under the circle). Type II: the plastomes of all samples of *G. leucocarpa* var. *yunnanensis*; the structure of samples LL61, LL63 and LL65 is denoted by the main circle and the remaining samples (LL59, LL66, X26, X27, X28, and X29), which contain an inversion, are indicated at upper right corner of the circle. Genes located outside the outer rim are transcribed in the counter clockwise direction, whereas genes inside are transcribed in the clockwise direction. The colored bars indicate different functional groups. The dashed gray area in the inner circle denotes the GC content of the corresponding genes. LSC: large single-copy region, SSC: small single-copy region, and IR: inverted repeat region.

Gaultheria ranged from 57 (*G. griffithiana*) to 75 (*G. longibracteolata*) (Table S3). The majority of the SSRs were mononucleotides (52.33%), followed by tetranucleotides (20.80%), trinucleotides (13.40%), dinucleotides (11.50%), and hexanucleotides (1.42%); the smallest number of SSRs were pentanucleotides (0.55%). No hexanucleotide repeats were detected in *G. griffithiana*, and pentanucleotide repeats were only detected in *G. longibracteolata*, *G. nummularioides*, and *G. sinensis* (Table S3).

The results of long-size repeat (>30 bp) analysis showed that there were only two types of repeats in the wintergreen samples: forward and reverse. The number of long repeats among the wintergreen plastomes ranged from 182 in *Gaultheria nummularioides* to 259 in *G. leucocarpa* var. *yunnanensis* (Fig. 4A). The maximum length of long repeats in each chloroplast ranged from 706 bp (e.g., *G. leucocarpa* var. *yunnanensis*-LL59) to 1722 bp (e.g., *G. fragrantissima*-LL27). A total of 9475 long repeats were detected in the 42 samples. There were 5321 long repeats with 30–50 bp in length, 2894 repeats of 51–100 bp, 989 repeats of 101–500 bp, 137

repeats of 501–1000 bp, and 134 repeats of 1001–2000 bp (Fig. 4A). The frequency of long repeats was a minimum of 2 repetitions and a maximum of 7 repetitions (Fig. 4B). The long repeats of the wintergreen plastomes were more frequently located in non-coding regions (e.g., *atpI-trnM*, *ndhf-trnV*, *ndhl-ndhG*, *pbf1-psbT*, *petD-petB*, *psal-trnM*, *psbB-psbJ*, *rpoA-rpoB*, *rps3-rpl16*, *rnn16-trnl*, *trnE-petA*, *trnM-rnn16*, *trnH-rpl23*, *trnI-rpl23*, *trnN-rps15*, *trnR-trnS*, *trn-petD*, *trnV-rps12*, and *ycf3-trnK*) than in coding regions (e.g., *infA*, *ndhA*, *ndhf*, *ndhl*, *petD*, *rpl22*, *rpl23*, *rpoA*, *rpoC1*, *rps14*, *rps3*, *trnM*, and *trnI*). Notably, we identified about 600 bp repeats located in both LSC and IR regions that covered the *trnM* and *rps14* genes, which resulted in two extra copies of these two genes in the IR regions (Fig. 4C).

3.4. Phylogenetic inference

The resulting ML and BI tree topologies were highly similar to one another. Our phylogenetic analysis using plastomes in which

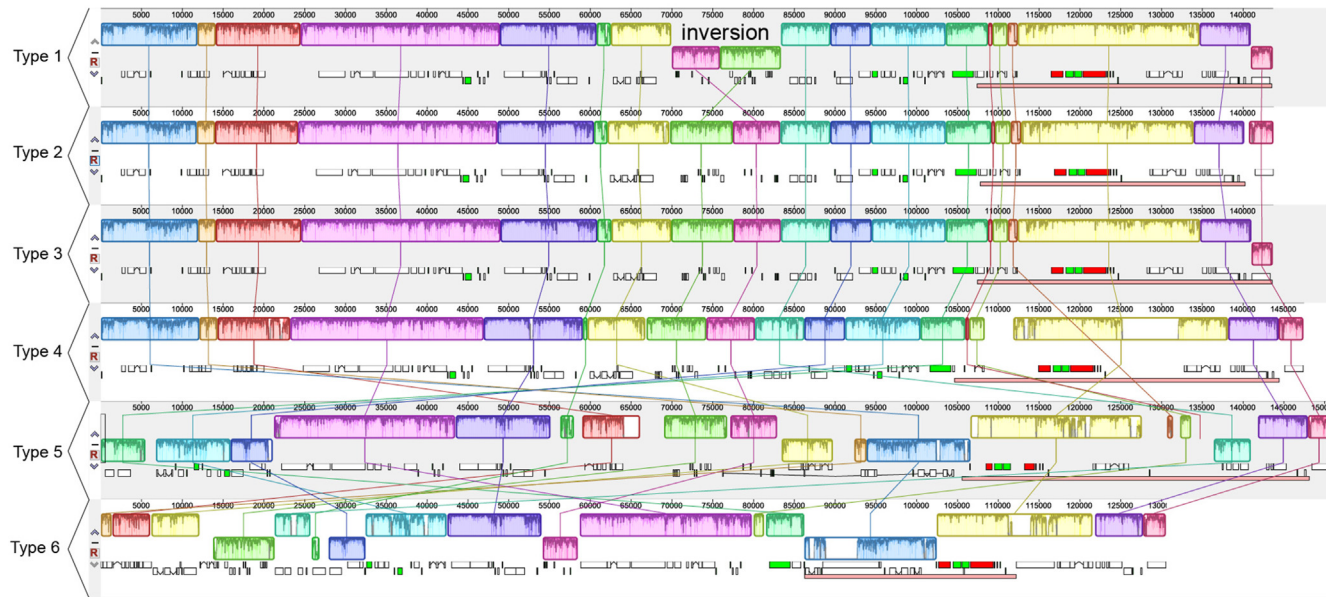


Fig. 3. Syntenies and rearrangements detected in the complete plastomes of nine Chinese medicinal wintergreens (*Gaultheria*) and the genera used for comparison from six related families within Ericales. Boxes of the same color connected with lines indicate the local collinear blocks and represent syntenic regions. Sequence identity similarity profiles are represented by histograms within each block, and sequences transcribed in reverse directions are indicated by the colored blocks above and below the center line. The taxa studied are divided into six types of plastome arrangements: Type 1, samples LL59, LL66, X26, X27, X28, and X29 of *G. leucocarpa* var. *yunnanensis*; Type 2, samples LL61, LL63, and LL65 of *G. leucocarpa* var. *yunnanensis*; Type 3, all samples of *G. fragrantissima*, *G. griffithiana*, *G. hookeri*, *G. longibracteolata*, *G. nummularioides*, *G. pyrolifolia*, *G. semi-infra*, and *G. sinensis*; Type 4, *Vaccinium* from Ericaceae; Type 5, *Rhododendron* from Ericaceae; and Type 6, genera studied from Pentaphylacaceae, Styracaceae, Primulaceae, Lecythidaceae, and Theaceae.

one of the IR copies was removed revealed that all samples of each wintergreen species clustered into a monophyletic group with moderate supports for *Gaultheria hookeri* (BS = 69, PP = 0.99) and *G. semi-infra* (BS = 87, PP = 1.00), and strong supports for seven other species (BS = 100, PP = 1.00; Fig. 5). *G. leucocarpa* var. *yunnanensis* was sister to the remaining eight wintergreen species. *G. sinensis* was sister, in turn, to a grade consisting of *G. griffithiana*, *G. pyrolifolia*, *G. longibracteolata*, *G. nummularioides*, *G. fragrantissima*, *G. semi-infra*, and *G. hookeri*.

3.5. Variation hotspots in the plastomes and candidate DNA barcodes for the Chinese medicinal wintergreens

We selected seven DNA regions (*incl.*, *infA*, *ndhF*, *psal-trnM*, *rps3-rpl16*, *trnQ-psaA*, *trnV-rps12*, and *ycf3-trnK*) with higher Pi values in the sliding window analyses, which were expected to have high potential for species delimitation in Chinese medicinal wintergreens (Fig. 6). We evaluated the fitness of these sequences as DNA barcoding regions by reconstructing ML phylogenetic trees (Figs. S1–S7). The results showed that the *trnV-rps12* region could discriminate all nine species successfully (BS ≥ 89). The *trnQ-psaA* region could discriminate eight out of nine species (BS ≥ 85), except for *Gaultheria hookeri*. The *ndhF* region could discriminate seven out of nine species (BS ≥ 96), except for *G. fragrantissima* and *G. hookeri*. The *ycf3-trnK* and *psal-trnM* region each could discriminate six out of nine species; specifically, the *ycf3-trnK* region could identify *G. griffithiana*, *G. leucocarpa* var. *yunnanensis*, *G. longibracteolata*, *G. nummularioides*, *G. pyrolifolia*, and *G. sinensis* (BS ≥ 95). The *psal-trnM* region had high resolution among *G. griffithiana*, *G. leucocarpa* var. *yunnanensis*, *G. longibracteolata*, *G. nummularioides*, *G. pyrolifolia* and *G. sinensis* (BS = 100). The *rps3-rpl16* region could discriminate five out of nine species: *G. griffithiana*, *G. leucocarpa* var. *yunnanensis*, *G. nummularioides*, *G. pyrolifolia*, and *G. sinensis* (BS ≥ 93). The *infA* region could discriminate only four out of nine species, i.e.,

G. fragrantissima, *G. leucocarpa* var. *yunnanensis*, *G. griffithiana*, and *G. sinensis* (BS ≥ 93).

4. Discussion

4.1. Gene content and structural variations of *Gaultheria* plastomes

The gene content of plastomes of land plants is generally considered to be conserved (Kumar et al., 2016), and the loss or duplication of different genes has been found in a variety of plants (Mohanta et al., 2020). It has been inferred that genes lost in plastomes may have moved to the nuclear genome or the function of these genes has been replaced by nuclear-encoded genes (Bryant et al., 2011; Savage et al., 2013; Mohanta et al., 2020). We identified several protein-coding gene losses and duplications in the *Gaultheria* plastomes. Both the *ycf1* and *ycf2* genes were absent in all studied *Gaultheria* samples. These two genes usually have elevated substitution rates and may have undergone pseudogenization in some land plant lineages (Oliver et al., 2010; Wolf et al., 2011). *ycf1* has also been found missing in grasses and some parasitic plants, and independent losses of the *ycf2* gene have occurred in multiple angiosperm groups, including Poaceae, Podostemaceae, Geraniaceae, and non-photosynthetic Ericaceae (Huang et al., 2010; Jin et al., 2020a). However, the mechanism for the loss of these two genes in the plastome is still not well understood.

In contrast to gene losses, gene duplications, attributed to repeat regions or IR expansions, were also detected in *Gaultheria* plastomes (*incl.*, *ndhF*, *rpl23*, *rps14*, and *trnM*). The *ndhF* gene was duplicated in all the samples of *G. leucocarpa* var. *yunnanensis* due to IR expansion. The chloroplast NAD(P)H dehydrogenase (*ndh*) complex is involved in photosystem I (PSI) cyclic electron transport and chlororespiration (Peng et al., 2011), and their mutation rates are high and sensitive to environmental conditions and stress (Silva et al., 2016). *G. leucocarpa* var. *yunnanensis* has a widespread

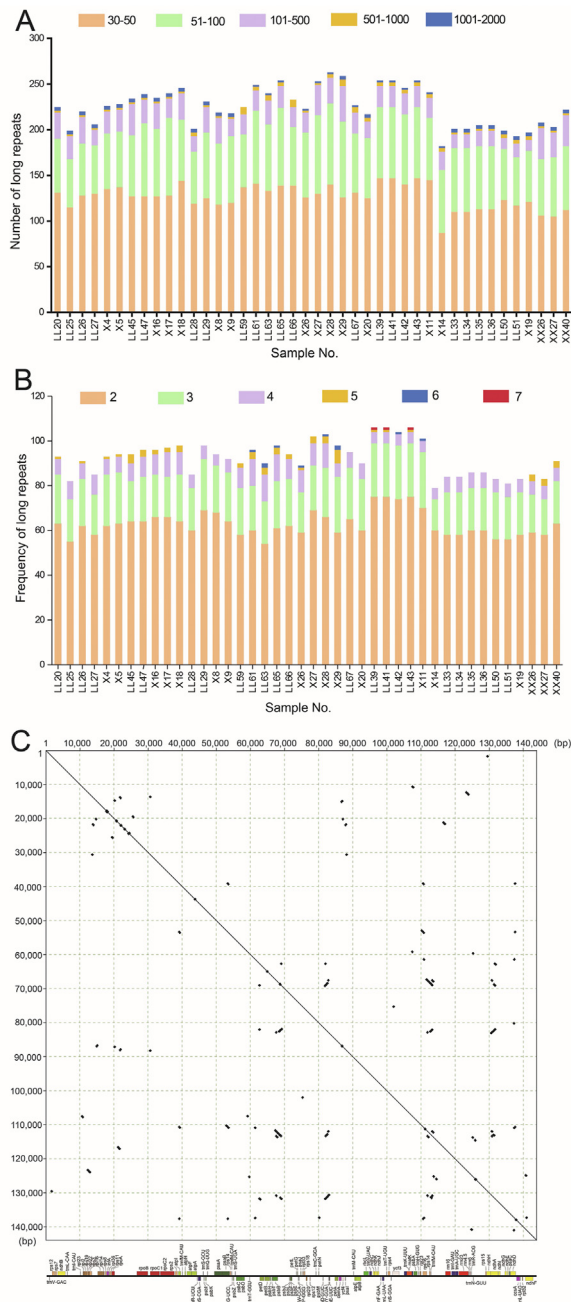


Fig. 4. Repeat sequences in Chinese medicinal wintergreen plastid genomes. (A) Number of long repeats by length; (B) Number of long repeats by frequency; (C) Self comparison of *Gaultheria* plastome (*G. fragrantissima*-LL20).

distribution in southern China, while other wintergreens inhabit the Himalaya-Hengduan regions. This difference in distribution implies that the duplication of *ndhF* gene is related to environmental adaptation in this species. In addition, plastomes with duplicated *ndh* genes usually exhibit extensive rearrangements and a higher frequency of pseudogenes (Martin et al., 1996; Casano et al., 2001; Paredes and Quiles, 2013). Consistent with this phenomenon, we identified an inversion in the LSC of some samples of *G. leucocarpa* var. *yunnanensis*.

It is rare that duplication of plastid genes does not involve movement of IR boundaries (Raubeson and Jansen, 2005; Bock,

2007; Guisinger et al., 2011). In fact, only a few instances have been documented, for example, the duplication of *clpP* gene in *Silene* L. and *Lychnis* L. (Erixon and Oxelman, 2008), the duplication of *psbj* and *trnI-CAU* in *Trachelium* Tourn. ex L. (Haberle et al., 2008), and the duplication of *rpl23* and three tRNA genes in *Jasminum* L. (Lee et al., 2006). In this study, we identified duplication of three genes (i.e., *rpl23*, *rps14* and *trnFM*) in *Gaultheria* plastomes that were independent of IR boundary shifts. The long repeats located in the LSC (between *psaB* and *trnG*) and both IR regions (between *rRN16* and *trnH*) that covered *rps14* and *trnFM* genes seemingly generated the three copies of these two genes. Additionally, we identified a fourth copy of *trnFM* in the LSC region adjacent to *atpI*, but with a slightly divergent sequence. By checking against other plastomes within Ericales, we inferred that the *rps14* and *trnFM* genes between *psaB* and *trnG* are likely the original copies. Similarly, the *rpl23* located in the LSC region (between *trnI* and *rpl2*) was not identical to the other two copies in the IR regions (between *trnH* and *rps16*); in this case, the LSC copy is likely the original copy.

Variation in plastome structure most typically involves expansion or contraction of the IRs into or out of adjacent single-copy regions (Ravi et al., 2008; Downie et al., 2015; Ye et al., 2018). The *trnN-GUU* gene is considered the ancestral IR/SSC endpoint that has been retained in most land plants, and the *trnV-GAC* gene represents the ancestral IR/LSC endpoint among most land plants (Zhu et al., 2016). Plastome IR expansions have been found in different plant groups, including Geraniaceae (Guisinger et al., 2011), Euphorbiaceae (Li et al., 2017), Solanaceae (Amirousefi et al., 2018), Bignoniacae (Thode and Lohmann, 2019) and Leguminosae (Bai et al., 2021). All plastomes of *Gaultheria fragrantissima*, *G. griffithiana*, *G. hookeri*, *G. longibracteolata*, *G. nummularioides*, *G. pyrolifolia*, *G. semi-infra* and *G. sinensis* expanded toward the SSC region from *trnN* to *rpl32*, and all samples of *G. leucocarpa* var. *yunnanensis* expanded toward the SSC region from *trnN* to *ndhF*. Different mechanisms have been proposed to explain IR expansions, such as gene conversion or double-strand DNA breaks (Goulding et al., 1996; Wang et al., 2008). In addition, some studies point out that the contraction and expansion of IR regions is a major contributor of plastomes size variation (Wang et al., 2018). For example, the IR regions of species from the genera *Acorus* and *Magnolia* are not expanded, and their plastome sizes are between 150 and 160 kb (Zhu et al., 2016), whereas the plastome size of Chinese medicinal wintergreens is between 176 and 182 kb. Our study validated that expansion of the IR region contributes to the increased genome size of *Gaultheria* species.

Similar to IR boundary shifts, inversions also represent essential mechanisms for plastome rearrangements, which contribute to the structural diversification of plant plastomes (Wicke et al., 2011; Jansen and Ruhlman, 2012). In nearly all photosynthetic land plants, plastomes are highly conserved in structural organization and gene arrangement (Jansen and Ruhlman, 2012; Zhu et al., 2016; Ye et al., 2018). Despite the commonly held view that plastomes have a conserved structure and sequence, they have been found to exhibit considerable variation in an increasing number of taxa (Wang et al., 2018; Ye et al., 2018). In our study, we found that there was one inversion in the LSC regions of six samples (LL59, LL66, X26, X27, X28 and X29) within *Gaultheria leucocarpa* var. *yunnanensis*, which disrupts the canonical order of the plastome genes. In addition, except for the inversion in the above samples in *G. leucocarpa* var. *yunnanensis*, we found that there were apparent multiple rearrangement events between the *Gaultheria* plastomes and those from the other five families (Lecythidaceae, Pentaphylacaceae, Primulaceae, Styracaceae and Theaceae) in Ericales. Our study provides new evidence of the variation between Ericales plastomes.

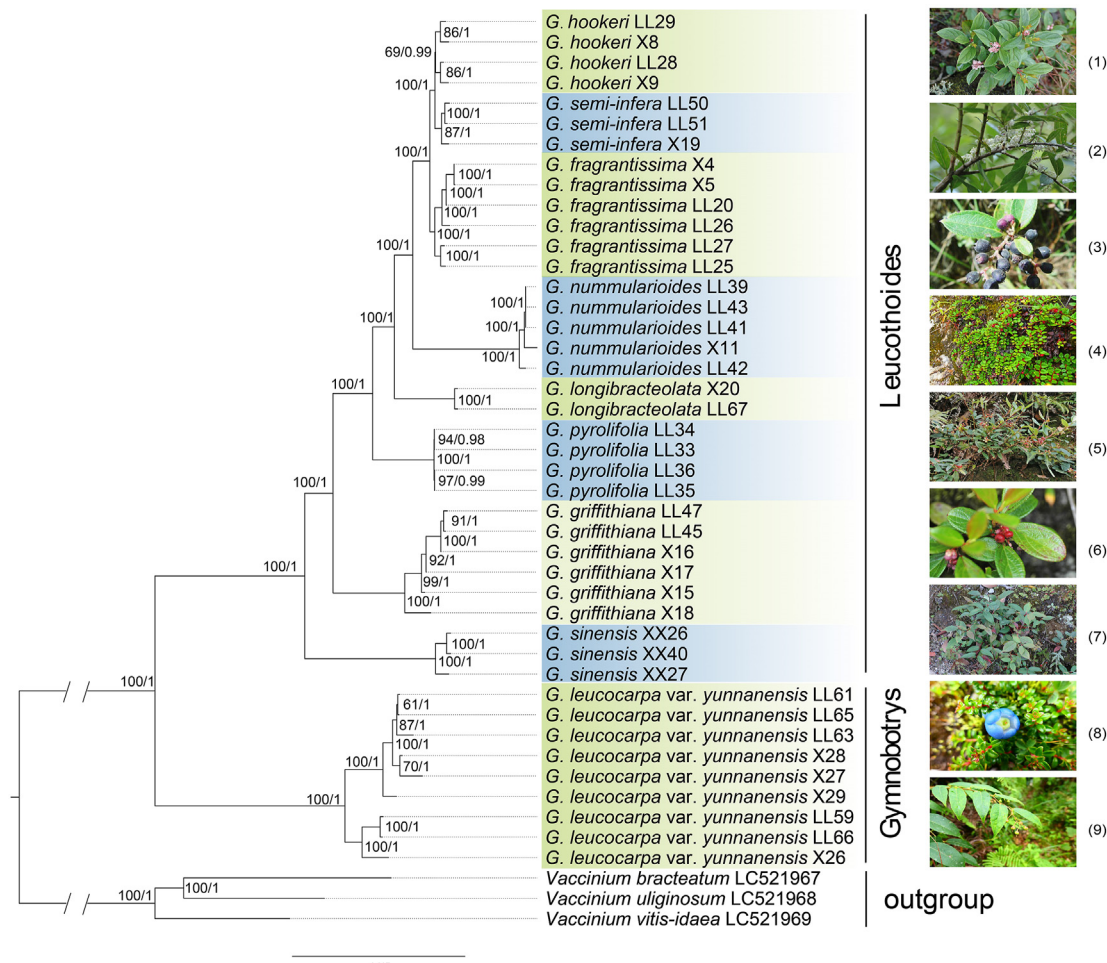


Fig. 5. A phylogenetic tree based on 42 plastome sequences of nine Chinese medicinal wintergreens (*Gaultheria*). Likelihood bootstrap support values (BS) and Bayesian posterior probability values (PP) are shown next to the nodes. Images on the right side show the plants of the nine species: (1) *G. hookeri*, (2) *G. semi-infra*, (3) *G. fragrantissima*, (4) *G. nummularioides*, (5) *G. longibracteolata*, (6) *G. pyrolifolia*, (7) *G. griffithiana*, (8) *G. sinensis*, and (9) *G. leucocarpa* var. *yunnanensis*.

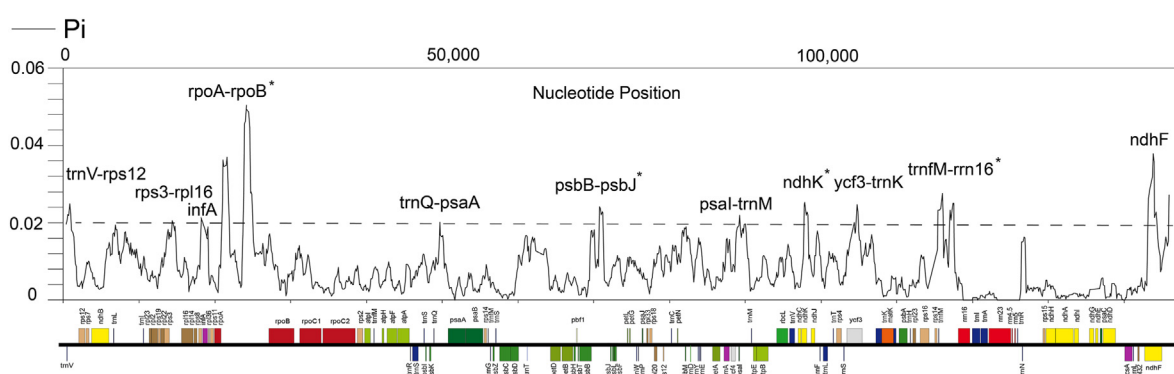


Fig. 6. Sliding window analysis of the complete plastomes of nine Chinese medicinal wintergreens (*Gaultheria*). X-axis: position of the window midpoint, Y-axis: nucleotide diversity within each window (window length: 600 bp, step size: 100 bp). Genic regions with π values > 0.2 are marked; region names with asterisk superscripts denote recommended DNA barcodes, while other regions are considered unsuitable for DNA barcodes due to the lack of either species discrimination or PCR amplification feasibility.

4.2. Abundant and variable repeat sequences

The long repeats of *Gaultheria* plastomes were characterized in terms of the number, length and distribution. Previous studies indicated that long repeats mainly occur in non-coding DNA sequences (Raubeson and Jansen, 2005). However, we detected long

repeats in coding regions of *Gaultheria* plastomes (e.g., *infA*, *ndhA*, *ndhF*, *ndhI*, *petD*, *rpl22*, *rpl23*, *rpl32*, *rpoA*, *rpoC1*, *rps14*, *rps3*, *trnfM*, and *trnL*). The most abundant sizes of long repeats among angiosperms are on average smaller than 50 bp (Raubeson and Jansen, 2005). With the increase in the number of plastomes sequenced, some longer repetitive sequences (approximately 100 bp) have also

been identified within some taxa. For example, the lengths of repeats range from 30 to 90 bp in Orchidaceae (Dong et al., 2018), 91 to 132 bp in Poaceae (Zhang et al., 2011), and 30 to 307 bp in Polypodiaceae (Liu et al., 2021). Generally, the number of repeats in the plastome is less than 50; for example, there are approximately 30 long repeats in *Cymbidium* (Yang et al., 2013), and 30 long repeats in *Debregeasia* (Wang et al., 2020). However, the longest long-repeat of each *Gaultheria* sample ranged from 706 bp to 1722 bp, and the number of long repeats was up to 259, which is significantly more abundant and variable than for many previously published plastomes.

Previous studies have shown that long repeats play a role in sequence rearrangement and variation in plastomes (Cavalier-Smith, 2002; Asano et al., 2004; Timme et al., 2007; Yang et al., 2013), and that large numbers of repeats can damage the stability of the plastome structure, for example, by producing inversions (Alexandre and Normand, 2010). Approximately 25 long repeats were located in the *psbB-psbJ* and *trnE-petA* regions of *Gaultheria* plastomes; thus, we speculate that this is one of the reasons for the 14-kb inversion in some samples of *G. leucocarpa* var. *yunnanensis*. Previous studies suggest that overall repeat content is positively correlated with the degree of genomic rearrangements (Wu et al., 2021b). This could be one of the reasons for the rearrangement of the plastomes in Ericaceae compared to other families within Ericales.

4.3. Phylogenetic relationships and delimitation of Chinese wintergreen species

Previous phylogenetic studies using a multiple-gene approach and international DNA barcoding (ITS, *Waxy*, *Lfy*, *matK*, *rbcL*, *rpl16*, *trnH-psbA*, *trnL-trnF* and *trnS-trnG*) failed to resolve the phylogenetic relationships among Chinese wintergreen species (Lu et al., 2010, 2019b; Ren et al., 2011). In this study, using plastomes in which one of the IR copies had been removed to reduce redundancy, we resolved the phylogenetic relationships among all nine Chinese medicinal wintergreens.

Previous phylogenetic analysis recovered three major clades in Chinese *Gaultheria*, i.e., the Leucothoides clade, the Trichophyllae clade, and the Gymnobotrys clade, with the Leucothoides clade sister to the Trichophyllae clade (Lu et al., 2019b). In this and other analyses, *G. leucocarpa* var. *yunnanensis*, which diverged earlier than other studied species, was resolved as a member within the Gymnobotrys clade; *G. fragrantissima*, *G. griffithiana*, *G. hookeri*, *G. longibracteolata*, *G. nummularioides*, *G. pyrolifolia* and *G. semi-infra* were placed within the Leucothoides clade, but with poorly supported infraspecific relationships, and *G. sinensis* was placed in the Trichophyllae clade (Lu et al., 2010, 2019a; Zhang et al., 2017). Our research supports this phylogeny, with *G. sinensis* sister to the grade comprising *G. fragrantissima*, *G. semi-infra*, *G. griffithiana*, *G. hookeri*, *G. nummularioides* and *G. longibracteolata*. We found that *G. nummularioides* had a sister relationship with the grade of *G. hookeri*, *G. semi-infra* and *G. fragrantissima*, and the clade comprising *G. hookeri*, *G. semi-infra* and *G. fragrantissima* was the most derived, which is consistent with the results of Lu et al. (2010). However, the relationship among the latter three species was poorly resolved in previous research (Lu et al., 2010; Fritsch et al., 2011), whereas our study suggests that each of the three species form a monophyletic lineage. In contrast to previous studies, we succeeded in clarifying the phylogenetic relationships among these nine species within the genus *Gaultheria*.

4.4. Candidate DNA barcodes

Chinese medicinal wintergreens are an important commodity in China, and the lack of genomic resources for *Gaultheria* has been

the main obstacle to taxonomical and genetic analysis, as well as identification and conservation. Common barcodes are not effective for these species (Lu et al., 2010; Ren et al., 2011); although plastomes have been successfully used as a plant super-barcode to distinguish these species, plastome super-barcodes are cost-prohibitive and require complex bioinformatics processing (Shen et al., 2019). Short DNA barcodes, or markers, may provide an effective and economical alternative for identification of target plants (Chase and Fay, 2009; Chen et al., 2010; Shen et al., 2019). Fortunately, the mutation events in plastomes are not randomly distributed within the sequence and are concentrated in certain 'hotspot' regions; therefore, specific barcodes or markers can be exploited from the plastome (Dong et al., 2012). In this study, we proposed eleven regions with high nucleotide variability (Pi) values that might have a high potential for species delimitation in Chinese medicinal wintergreens. These mutational hotspots have the potential to resolve taxonomic issues in the genus and to be used in the future as barcodes for species identification. An ideal DNA barcode should be easily retrievable with a universal primer pair, an appropriately short sequence length to facilitate DNA extraction and amplification (Shen et al., 2019). The intergenic regions *psbB-psbJ* and *trnM-psbM* possess high nucleotide variability (Pi) values, however, their PCR success rates were rather low (8.3% and 0 for each, respectively; tested with six samples of each wintergreen by using four primer pairs); thus, these two regions were excluded for the consideration of DNA barcodes. The *rpoA-rpoB* region was too long (approximately 6500 bp) for Sanger sequencing. Therefore, we finally selected seven regions (*infA*, *ndhF*, *psaI-trnM*, *rps3-rpl16*, *trnQ-psaA*, *trnV-rps12* and *ycf3-trnK*) that have the potential to develop into DNA barcodes. Our results show that the *trnV-rps12* region provided the best resolution for identifying all nine species of Chinese medicinal wintergreens. It was followed by *trnQ-psaA* region, which identified eight out of nine species. The *infA* gene provides the least resolution, which allowed the identification of only four out of nine species. In addition, eight divergence hotspot regions, including *rpl36-infA*, *trnF* (GAA)-*ndhJ*, *trnD* (GUC)-*psbM*, *trnL* (UAA)-*trnF* (GAA), *trnT* (UGU)-*trnL* (UAA), *rpl23b*, *rps3b* and *petN-trnC* (GCA), were recommended as candidate DNA barcodes for species identification of the Trichophyllae clade (Zhang et al., 2017). In summary, different sets of DNA barcodes were detected for delimitation of species from the Trichophyllae clade and the Leucothoides clade.

5. Conclusions

Our research showed that the complete plastome could be used as a plant super-barcode to distinguish closely related medicinal wintergreens successfully, and that even specific molecular markers can be screened based on plastome sequences to distinguish the species. In addition, several unique characteristics of plastomes in *Gaultheria*, such as the loss of genes, rare gene duplication events, inversions (within *G. leucocarpa* var. *yunnanensis*), multiple rearrangement events, and remarkably long repeats, reveal new perspectives for understanding the dynamics of angiosperm plastomes. Furthermore, reticulate hybridization or species radiation that may have occurred during the evolutionary history of *Gaultheria* was not revealed by plastome sequence data, and further studies with increased taxa sampling and nuclear DNA sequences are necessary.

Author contributions

LL and XYD conceived the work. YLX performed the experiments and analyses. HHS contributed materials/analysis tools. YLX

- Luo, B.S., Gu, R.H., Kennelly, E.J., et al., 2018. *Gaultheria* ethnobotany and bioactivity: blueberry relatives with anti-inflammatory, antioxidant, and anticancer constituents. *Curr. Med. Chem.* 25, 5168–5176.
- Luo, B.S., Kastrat, E., Morcol, T., et al., 2021. *Gaultheria longibracteolata*, an alternative source of wintergreen oil. *Food Chem.* 342, 128244.
- Lv, S.Y., Ye, X.Y., Li, Z.H., et al., 2022. Testing complete plastomes and nuclear ribosomal DNA sequences for species identification in a taxonomically difficult bamboo genus *Fargesia*. *Plant Divers.* <https://doi.org/10.1016/j.pld.2022.04.002>. In press.
- Ma, X., Zhao, L., Han, Z., et al., 2002. Comparison of the contents of lignans glycosides in 5 medicinal plants of *Gaultheria* by HPLC. *J. Plant Resour. Environ.* 11, 2.
- Ma, X.J., Zhao, L., Du, C.F., et al., 2001. Advances in studies on *Gaultheria leucocarpa* var. *yunnanensis* and medicinal plants of *Gaultheria* L. *Chin. Trad. Herb. Drugs* 32, 5.
- Martin, M., Casano, L.M., Sabater, B., 1996. Identification of the product of *ndhA* gene as a thylakoid protein synthesized in response to photooxidative treatment. *Plant Cell Physiol.* 37, 293–298.
- Mohanta, T.K., Mishra, A.K., Khan, A., et al., 2020. Gene loss and evolution of the plastome. *Genes* 11, 1133.
- Moore, M.J., Dhingra, A., Soltis, P.S., et al., 2006. Rapid and accurate pyrosequencing of angiosperm plastid genomes. *BMC Plant Biol.* 6, 1–13.
- Mukhopadhyay, M., Bantawa, P., Mondal, T.K., et al., 2016. Biological and phylogenetic advancements of *Gaultheria fragrantissima*: economically important oil bearing medicinal plant. *Ind. Crop. Prod.* 81, 91–99.
- Mwanza, V.M., He, D.X., Gichira, A.W., et al., 2020. The complete plastome sequences of five *Aponogeton* species (Aponogetonaceae): insights into the structural organization and mutational hotspots. *Plant Divers.* 42, 334–342.
- Nguyen, L.T., Schmidt, H.A., Von Haeseler, A., et al., 2015. IQ-TREE: a fast and effective stochastic algorithm for estimating maximum-likelihood phylogenies. *Mol. Biol. Evol.* 32, 268–274.
- Nikolić, M., Marković, T., Mojović, M., et al., 2013. Chemical composition and biological activity of *Gaultheria procumbens* L. essential oil. *Ind. Crop. Prod.* 49, 561–567.
- Oliver, M.J., Murdock, A.G., Mishler, B.D., et al., 2010. Chloroplast genome sequence of the moss *Tortula ruralis*: gene content, polymorphism, and structural arrangement relative to other green plant chloroplast genomes. *BMC Genomics* 11, 1–8.
- Paredes, M., Quiles, M.J., 2013. Stimulation of chlороrespiration by drought under heat and high illumination in *Rosa meillandina*. *J. Plant Physiol.* 170, 165–171.
- Peng, L., Yamamoto, H., Shikanai, T., 2011. Structure and biogenesis of the chloroplast NAD(P)H dehydrogenase complex. *Biochim. Biophys. Acta, Bioenerg.* 1807, 945–953.
- Raubeson, L.A., Jansen, R.K., 2005. Chloroplast genomes of plants. *Plant Diversity and Evolution: Genotypic and Phenotypic Variation in Higher Plants*. CABI, Cambridge, pp. 45–68.
- Ravi, V., Khurana, J., Tyagi, A., et al., 2008. An update on chloroplast genomes. *Plant Syst. Evol.* 271, 101–122.
- Ren, H., Lu, L., Wang, H., et al., 2011. DNA barcoding of *Gaultheria* L. in China (Ericaceae: Vaccinioideae). *J. Syst. Evol.* 49, 411–424.
- Ronquist, F., Teslenko, M., Van Der Mark, P., et al., 2012. MrBayes 3.2: efficient Bayesian phylogenetic inference and model choice across a large model space. *Syst. Biol.* 61, 539–542.
- Savage, L.J., Imre, K.M., Hall, D.A., et al., 2013. Analysis of essential *Arabidopsis* nuclear genes encoding plastid-targeted proteins. *PLoS One* 8, e73291.
- Shen, Z., Lu, T., Zhang, Z., et al., 2019. Authentication of traditional Chinese medicinal herb "Gusuibu" by DNA-based molecular methods. *Ind. Crop. Prod.* 141, 111756.
- Silva, S.R., Diaz, Y.C., Penha, H.A., et al., 2016. The chloroplast genome of *Utricularia reniformis* sheds light on the evolution of the *ndh* gene complex of terrestrial carnivorous plants from the Lentibulariaceae family. *PLoS One* 11, e0165176.
- Stamatakis, A., 2014. RAxML version 8: a tool for phylogenetic analysis and post-analysis of large phylogenies. *Bioinformatics* 30, 1312–1313.
- Thode, V.A., Lohmann, L.G., 2019. Comparative chloroplast genomics at low taxonomic levels: a case study using *Amphilophium* (Bignonieae, Bignoniacae). *Front. Plant Sci.* 10, 796.
- Timme, R.E., Kuehl, J.V., Boore, J.L., et al., 2007. A comparative analysis of the *Lactuca* and *Helianthus* (Asteraceae) plastid genomes: identification of divergent regions and categorization of shared repeats. *Am. J. Bot.* 94, 302–312.
- Wang, R.J., Cheng, C.L., Chang, C.C., et al., 2008. Dynamics and evolution of the inverted repeat-large single copy junctions in the chloroplast genomes of monocots. *BMC Evol. Biol.* 8, 1–14.
- Wang, R.N., Milne, R.I., Du, X.Y., et al., 2020. Characteristics and mutational hotspots of plastomes in *Debregeasia* (Urticaceae). *Front. Genet.* 11, 729.
- Wang, Y., Wang, S., Liu, Y., et al., 2021. Chloroplast genome variation and phylogenetic relationships of *Atractylodes* species. *BMC Genomics* 22, 1–12.
- Wang, Y.H., Wicke, S., Wang, H., et al., 2018. Plastid genome evolution in the early-diverging legume subfamily Cercidoideae (Fabaceae). *Front. Plant Sci.* 9, 138.
- Wick, R.R., Schultz, M.B., Zobel, J., et al., 2015. Bandage: interactive visualization of de novo genome assemblies. *Bioinformatics* 31, 3350–3352.
- Wicke, S., Schneeweiss, G.M., Depamphilis, C.W., et al., 2011. The evolution of the plastid chromosome in land plants: gene content, gene order, gene function. *Plant Mol. Biol.* 76, 273–297.
- Williams, A.V., Miller, J.T., Small, I., et al., 2016. Integration of complete chloroplast genome sequences with small amplicon datasets improves phylogenetic resolution in *Acacia*. *Mol. Phylogenet. Evol.* 96, 1–8.
- Wolf, P.G., Der, J.P., Duffy, A.M., et al., 2011. The evolution of chloroplast genes and genomes in ferns. *Plant Mol. Biol.* 76, 251–261.
- Wu, H., Ma, P.F., Li, H.T., et al., 2021a. Comparative plastomic analysis and insights into the phylogeny of *Salvia* (Lamiaceae). *Plant Divers.* 43, 15–26.
- Wu, S., Chen, J., Li, Y., et al., 2021b. Extensive genomic rearrangements mediated by repetitive sequences in plastomes of *Medicago* and its relatives. *BMC Plant Biol.* 21, 1–16.
- Yang, J.B., Tang, M., Li, H.T., et al., 2013. Complete chloroplast genome of the genus *Cymbidium*: lights into the species identification, phylogenetic implications and population genetic analyses. *BMC Evol. Biol.* 13, 1–12.
- Ye, W.Q., Yap, Z.Y., Li, P., et al., 2018. Plastome organization, genome-based phylogeny and evolution of plastid genes in Podophyloideae (Berberidaceae). *Mol. Phylogenet. Evol.* 127, 978–987.
- Zhang, M.Y., Fritsch, P.W., Ma, P.F., et al., 2017. Plastid phylogenomics and adaptive evolution of *Gaultheria* series *Trichophyllae* (Ericaceae), a clade from sky islands of the Himalaya-Hengduan Mountains. *Mol. Phylogenet. Evol.* 110, 7–18.
- Zhang, Y., Li, J., He, F., et al., 2020. Chemical constituents of *Gaultheria leucocarpa* var. *yunnanensis* (Franch.) T.Z. Hsu & R.C. Fang. *Centr. South Pharm.* 18, 1800–1802.
- Zhang, Y.J., Ma, P.F., Li, D.Z., 2011. High-throughput sequencing of six bamboo chloroplast genomes: phylogenetic implications for temperate woody bamboos (Poaceae: Bambusoideae). *PLoS One* 6, e20596.
- Zhu, A., Guo, W., Gupta, S., et al., 2016. Evolutionary dynamics of the plastid inverted repeat: the effects of expansion, contraction, and loss on substitution rates. *New Phytol.* 209, 1747–1756.